The WIRED Survey. IV. New Dust Disks from the McCook & Sion White Dwarf Catalog

D. W. Hoard[1,2,3], John H. Debes[4], Stefanie Wachter[1], David T. Leisawitz[5], and Martin Cohen[6]

ABSTRACT

We have compiled photometric data from the *Wide-field Infrared Survey Explorer* All Sky Survey and other archival sources for the more than 2200 objects in the original McCook & Sion Catalog of Spectroscopically Identified White Dwarfs. We applied color-selection criteria to identify 28 targets whose infrared spectral energy distributions depart from the expectation for the white dwarf photosphere alone. Seven of these are previously known white dwarfs with circumstellar dust disks, five are known central stars of planetary nebulae, and six were excluded for being known binaries or having possible contamination of their infrared photometry. We fit white dwarf models to the spectral energy distributions of the remaining ten targets, and find seven new candidates with infrared excess suggesting the presence of a circumstellar dust disk. We compare the model dust disk properties for these new candidates with a comprehensive compilation of previously published parameters for known white dwarfs with dust disks. It is possible that the current census of white dwarfs with dust disks that produce an excess detectable at K-band and shorter wavelengths is close to complete for the entire sample of known WDs to the detection limits of existing near-IR all-sky surveys. The white dwarf dust disk candidates now being found using longer wavelength infrared data are drawn from a previously underrepresented region of parameter space, in which the dust disks are overall cooler, narrower in radial extent, and/or contain fewer emitting grains.

Subject headings: circumstellar matter — planetary systems — surveys — white dwarfs

[1]Max Planck Institut für Astronomie, Heidelberg, 69117, Germany

[2]Visiting Scientist, MPIA; email: `hoard@mpia.de`

[3]Eureka Scientific, Inc., Oakland, CA 94602, USA

[4]Space Telescope Science Institute, Baltimore, MD 21218, USA

[5]Goddard Space Flight Center, Greenbelt, MD 20771, USA

[6]Monterey Institute for Research in Astronomy, Marina, CA 93933, USA

arXiv:1304.7801v2 [astro-ph.GA] 3 May 2013

1.   Introduction

Dust disks are common in a wide variety of astrophysical situations, including the central engines of quasars and active galactic nuclei (e.g., Rowan-Robinson 1977; Antonucci 1993), the precursors of planetary system formation around protostars (e.g., Natta 2008) and post-formation debris around young stars (e.g., Aumann 1985; Chini et al. 1991), and even the recently discovered largest ring of Saturn (e.g., Verbiscer et al. 2009). The first dust disk around a white dwarf (WD), G29-38, was discovered by virtue of its infrared (IR) excess over the WD photosphere (Zuckerman & Becklin 1987), although it took another decade to cast aside all doubts that the excess was truly due to dust and not an unresolved brown dwarf companion (Koester et al. 1997; Kuchner et al. 1998). Debes & Sigurdsson (2002) and Jura (2003) developed a model for the origin of WD dust disks involving tidal disruption of a comet or asteroid perturbed into the WD Roche lobe due to the gravitational influence of a remnant planetary system containing at least one massive planet (Debes et al. 2012). It wasn't until 2005 that the second WD with a dust disk, GD 362, was discovered (Becklin et al. 2005; Kilic et al. 2005). By the end of 2010, 20 dusty WDs were known (Table 5.1 in Farihi 2011), largely owing to sensitive IR observations from the *Spitzer Space Telescope*.

Predating the discovery of dust around WDs, it was known that a small fraction of WDs show absorption lines of metals in their optical and UV photospheric spectra (e.g., Lacombe et al. 1983; Shipman & Greenstein 1983; Zeidler-K.T. et al. 1986). These lines originate from "pollution" of a WD's geometrically thin, high density (but non-degenerate) atmosphere, which in most objects is otherwise pure hydrogen or helium. Gravitational settling times in hydrogen-rich (DA) WD atmospheres are very short (a few days to $\lesssim 1000$ yr), so metals quickly diffuse out of the photosphere unless replenished. Thus, the observed metals were thought to be supplied by ongoing accretion from the ISM (Sion et al. 1990). This explanation was problematic; notably, the required accretion rate is high ($\gtrsim 10^{8.5}$ g s^{-1} compared to $\sim 10^7$ g s^{-1} expected from ISM accretion) and it is difficult to explain the relative elemental abundances of the accreted material, which do not match equilibrium ISM values (see Farihi et al. 2010 and the review and discussion in Sections 5.2.4 and 5.6.6 of Farihi 2011).

It is a testament to the strength of the asteroid disruption model for WD dust disks that it also explains the metal-rich WDs, via accretion from circumstellar dust. Zuckerman et al. (2007) showed that the relative abundances of accreted metals in the dusty WD GD 362 closely match those of the terrestrial planets. Analyses of two metal polluted WDs (GD 61, NLTT 43806) suggest that the accreted dust derived from an asteroid whose origin was in the outer layers of a differentiated planet, in which the heaviest elements had sunk to the core, leaving a lithosphere rich in Ca and possibly water (Farihi et al. 2011; Zuckerman et al. 2011). Thus, observing WDs with dust disks is directly linked to determining how the chemical diversity of planetary systems can influence the probability that some planets support life.

In order to facilitate this, a large sample of WDs with dust disks is desired. Consequently,

we have been carrying out the *WISE* InfraRed Excesses around Degenerates (WIRED) Survey, utilizing photometry from the *Wide-field Infrared Survey Explorer* (*WISE*), a NASA medium class Explorer mission launched on 14 Dec 2009 (Wright et al. 2010). *WISE* mapped the entire sky at 3.4, 4.6, 12, and 22 μm (W1, W2, W3, and W4 bands, respectively) with 5σ point source sensitivities of approximately 0.08, 0.11, 1, and 6 mJy, respectively. Complete sky coverage was achieved in mid-July 2010. The WIRED Survey has the goals of characterizing WD stars in the *WISE* bands, confirming objects known to have IR excess from past observations (*Spitzer*, 2MASS, UKIDSS, etc.), and revealing new examples of WDs with IR excess that can be attributed to unresolved companions or circumstellar debris disks. We are utilizing target lists drawn from cataloged WD samples (e.g., from the Sloan Digital Sky Survey, McCook & Sion, etc.). To date, we have published results from WIRED for the SDSS WD sample that have nearly tripled the number of known WDs with circumstellar dust disks and increased the number of WD + brown dwarf binaries by almost an order of magnitude. We now present initial results from examining the McCook & Sion (1999) (henceforth, MS99) catalog of spectroscopically identified WDs, which resulted in the new identification of seven WDs with IR excess indicating the likely presence of a circumstellar dust disk.

2. Targets and Data

MS99 contains 2249 (optical) spectroscopically identified WDs. The updated and online version of MS99, the Villanova University White Dwarf Catalog[1] (henceforth, MSonline) currently contains over 14,000 entries. For our purposes, we have used only those targets contained in the original print publication of MS99 (most of the new WDs listed in MSonline are objects discovered by SDSS and are covered in our previous WIRED paper; see Debes et al. 2011). Since the publication of MS99, a number of the WDs were subsequently reclassified as non-WDs (e.g., quasars) or nonexistent (e.g., some WDs are listed twice in MS99 with different names, such as WD 2321-549 = WD J2324-546), leaving 2202 viable targets. To further narrow the target list, we considered only the 1474 WDs from MS99 for which Hoard et al. (2007) found 2MASS near-IR detections.

As a first pass at identifying IR-bright (or otherwise "interesting") WDs from this input list, we utilized the following selection criteria for each target: (1) 2MASS-J, W1, and W2 photometry exists, (2) the *WISE* color index (W1−W2) $\geq$ +0.3 mag, and (3) the signal-to-noise ratios of the W1 and W2 detections are both $\geq$ 7.

The IR color-color diagram of the MS99 WDs (see Figure 1) demonstrates that the 2nd criterion selects the majority of known dusty WDs, while avoiding the bulk of the "uninteresting" WDs. The 3rd criterion excludes color-selected targets whose redness is spurious, resulting from low S/N photometry. A broad 10 μm silicate emission feature is a hallmark of circumstellar dust around

---

[1]See http://www.astronomy.villanova.edu/WDCatalog/index.html.

WDs (Jura et al. 2009) and falls into the W3 band. In principle, this could offer an additional selection criterion for identifying WDs with dust. In practice, however, we found that due to the lower sensitivity of *WISE* in the W3 band compared to W1 and W2 (cf. while 67% and 58% of our input sample have a W1 and/or W2 detection, respectively, only 16% have a W3 detection), almost 92% of the targets that have a cataloged W3 detection are already selected by our 1st criterion. Only two of the targets with a W3 detection that were *not* selected by our 1st criterion have S/N ≥ 7 in W3, and both of them are unusable: WD 1919+145 is contaminated by a nearby source (Mullally et al. 2007) and WD 2110+300 is in an unresolved binary with a G-type giant star (ζ Cygni; Griffin & Keenan 1992). In addition, closer inspection of the *WISE* images of our targets shows that as many as ∼50% of the cataloged W3 "detections" (especially at low S/N) are probably unreliable (e.g., due to bright, structured background or nearby sources) and should be treated as upper limits (e.g., see Section 2.1).

Incidentally, there are some features of the IR color-color diagram that we will not discuss in detail, but are worth noting:

- There are two principal loci of WDs (plotted as small gray circles): a large one centered around (J−W1) ≈ −0.25 mag, (W1−W2) ≈ 0 mag, and a smaller one at (J−W1) ≈ +1.0 mag, (W1−W2) ≈ +0.2 mag. The former is the locus of "naked" WDs, while the latter is the locus of unresolved binaries containing a WD and a low mass main sequence star. We found a similar distribution of the majority of points in the r, i, J, W1, W2 color-color planes for the targets selected from the SDSS Data Release 7 preliminary WD catalog (Debes et al. 2011).

- The known WDs with circumstellar dust disks form a broad sequence extending from the locus of naked WDs (with blue colors) to the upper right (red) corner of the color-color diagram. The new candidate WDs with dust disks reported here (see below) follow this sequence at the red end, and broaden it at the blue end.

Our criteria initially resulted in the selection of 28 WDs from the MS99 sample. Seven of these were excluded because they are known WDs with circumstellar dust disks: WD 0408-041 (Kilic et al. 2006), WD 0843+516 (Gänsicke et al. 2012), WD 1015+161 (Jura et al. 2007a), WD 1116+026 (Jura et al. 2007a), WD 1150-153 (Kilic & Redfield 2007), WD 1541+650 (Kilic et al. 2012), and WD 1729+371 (Becklin et al. 2005; Kilic et al. 2005). Five WDs were excluded for being known central stars of planetary nebulae (CSPNs): WD 0558-756 (Henize & Fairall 1981; Rauch & Werner 1993), WD 0950+139 (Liebert et al. 1989), WD 1821+643 (Starrfield et al. 1985), WD 1958+015 (Napiwotzki & Schoenberner 1995), and WD 2333+301 (Schoenberner & Napiwotzki 1990). Another six were rejected for various reasons related to contamination of their photometry:

- WD 0457-103 is in a known spectroscopic binary with a bright G–K star (63 Eri; Shara et al. 1997; Barstow et al. 1994); it remains unresolved despite a high resolution *Hubble Space Telescope* imaging investigation (Barstow et al. 2001).

- WD 0725+318 has a nearby source (RA=07:28:11.65, dec=+31:43:46.57, J2000), which is revealed in the SDSS images of the field as a red background galaxy that is very bright in the IR and likely contaminates the WD photometry in both 2MASS and *WISE*.

- WD 1109-225 is in a known unresolved spectroscopic binary with a bright A star (β Crt; Fleming et al. 1991).

- WD 1201+437 is classified as a DC+dMe binary by Fleming et al. (1993). Xu et al. (1999) classify it as a quasar based on its X-ray properties; however, we note that their X-ray error circle has a $9''$ radius, so this could be a mis-identification. In either case, we would remove it from our sample.

- WD 1235+321 has a stellar profile in the *WISE* images that is faint and extended, while the SDSS images show two nearby faint point sources that are likely contaminating the *WISE* photometry. These sources are: a star located $5.6''$ west with i = 20.11 mag and z = 19.94 mag, and a galaxy located $6.2''$ east with i = 19.87 mag and z = 19.64 mag. There are three additional faint sources within $13''$ of the WD (two to the south, one to the southwest in the direction of the bright star located $25''$ southwest of the WD), all with i > 21 mag and z > 22 mag.

- WD 1859+429 is in a wide binary with a common proper motion companion located $\approx 15''$ to the northeast. The common proper motion companion is not problematic; however, due to its proper motion, the WD is superposed on a field star in the 2MASS images. It is likely that this star contaminates the *WISE* photometry.

This leaves 10 WDs that we classified as targets-of-interest and for which we constructed UV–IR spectral energy distributions (SEDs). In addition to the 2MASS (Skrutskie et al. 2006) All Sky Data Release Point Source Catalog and *WISE* All Sky Release[2] photometry, we utilized photometric data from the *Galaxy Evolution Explorer* (*GALEX*; Martin et al. 2005), the Sloan Digital Sky Survey (SDSS Data Release 7; Abazajian et al. 2009), the AAVSO Photometric All Sky Survey (APASS Data Release 6)[3], and the *Spitzer Space Telescope* Enhanced Imaging Products Source List (Cryogenic Release v2.0, January 2013)[4]. For the purpose of modeling the SEDs, we converted the various photometric measurements from magnitudes into flux densities using published zero points for each photometric band (Bessell 1979; Skrutskie et al. 2006; Abazajian et al. 2009; Wright et al. 2010). All of the photometric data for the targets-of-interest plus the CSPNs and known WDs with dust disks, along with published spectral types, effective temperatures, and surface gravities of the WDs, are listed in Tables 1–3.

---

[2]See the Explanatory Supplement at `http://wise2.ipac.caltech.edu/docs/release/allsky/expsup/`.

[3]See `http://www.aavso.org/apass`.

[4]See the Explanatory Supplement at
`http://irsa.ipac.caltech.edu/data/SPITZER/Enhanced/Imaging/docs/Spitzer_EIP_expsup.pdf`.

We then fit either a DA or DB model, as appropriate for the published WD type, to the UV–optical–near-IR (JHK) portion of the target SEDs, using grids of H- and He-rich WD cooling models (kindly provided by P. Bergeron) that include the *GALEX*, SDSS, Johnson UBVRI, 2MASS, and *WISE* bands (Bergeron et al. 1995; Holberg & Bergeron 2006). The published WD temperature and log g values from Table 1 were used as initial values (a "typical" value of log g = 8.0 was assumed in cases for which there is no published value). We searched for best-fitting models within the 1σ uncertainties of the literature values of $T_{\rm eff}$ and log g. For WDs with no published uncertainty for $T_{\rm eff}$, we assumed ±2000 K.

Seven of the targets have an obvious excess over the WD model in the IR. For these objects, we re-fit the entire SED using an additional circumstellar dust disk component. The model dust disk SED was calculated as originally devised by Jura (2003), following the procedure described in Debes et al. (2011), with free parameters of inner radius, width, and inclination. The minimum allowed inner disk radius was given by a conservative sublimation temperature of $T_{\rm subl} = 2100$ K; in the case of our hottest WD (WD 0420+520, $T_{\rm eff} = 24300$ K), we relaxed this criterion to $T_{\rm subl} = 2500$ K in order to obtain the best dust disk model fit[5].

As noted above, the broad 10 μm silicate emission feature that is commonly seen in the IR spectra of WDs with circumstellar dust (Jura et al. 2009) could contribute in the W3 band; consequently, we did not use the W3 photometry to constrain the models. Any model that is too faint at W3 indicates the presence of a silicate emission feature or a significant amount of cool dust at large distances from the WD. If the model is too bright at W3, then this likely indicates that the assumed outer radius of the disk is too large. The silicate emission feature at 18–20 μm (e.g., seen in the IR spectrum of the archetype dusty WD G29-38 = WD 2326+049; Reach et al. 2009) is generally weaker in amplitude but broader than the 10 μm feature (Papoular & Pegourie 1983; Thompson et al. 2003; Jura et al. 2007b)[6], and could contribute in the W4 band. The disk inclinations are generally poorly constrained by the models. The SEDs and model fits are shown in Figure 2; the WD and dust disk model parameters are listed in Table 4. These seven objects are our new candidate WDs with dust disks.

There are three reduced chi-squared ($\tilde{\chi}^2$) values listed in Table 4 for each model. These provide different measurements of the goodness of the model fit:

- The parameter $\tilde{\chi}^2_{\rm wd}$ refers to the goodness of just the WD model component compared to only the UV–optical–near-IR (JHK) data. In this wavelength region, we expect generally

---

[5]Silicate dust, for example, is generally assumed to sublimate at $T \gtrsim 1500$–2000 K (e.g., Pollack et al. 1994; Kobayashi et al. 2011); however, Rafikov & Garmilla (2012) recently calculated that due to the high metal vapor pressure at the inner edge of WD dust disks, the dust grain sublimation temperatures can be 300–400 K higher than is generally assumed, and the inner edge of the disk can be superheated to as high as 2500–3500 K.

[6]Laboratory experiments suggest that "fresh" silicates have a very large 10/20 μm flux ratio, but factors such as metal content or oxidation – that is, age – of the silicate compounds can increase the strength of the 20 μm feature relative to the 10 μm feature (Nuth & Hecht 1990). Dust temperature can also affect this ratio (Suh 1999).

good agreement with a "naked" WD model even in the presence of circumstellar dust (which contributes most strongly at mid-IR and longer wavelengths). Large values of this statistic likely indicate deviations from the WD model in the UV; the *GALEX* data are typically among the brightest points in the SED and have very small relative errors. If $\tilde{\chi}^2_{\rm wd}$ is large because of deviations in the UV, then the values of the other two $\tilde{\chi}^2$ statistics will also be large, as the errors are dominated by the poor fit in the UV. For example, removing the two UV points from the WD 2329+407 SED reduces $\tilde{\chi}^2_{\rm wd}$ from 107 to 2.1 and $\tilde{\chi}^2_{\rm disk}$ (see below) from 94 to 2.6. In the case of WD 1046-017, removing the UV points causes all of its $\tilde{\chi}^2$ values to drop to ≈ 1.4.

- The parameter $\tilde{\chi}^2_{\rm all}$ refers to the goodness of just the WD model component compared to all of the available photometric data. Large values (e.g., $\tilde{\chi}^2_{\rm all} > \tilde{\chi}^2_{\rm wd} > 1$) indicate the need for an additional model component in the IR.

- The parameter $\tilde{\chi}^2_{\rm disk}$ refers to the goodness of the WD + dust disk model compared to all of the available photometric data. If $\tilde{\chi}^2_{\rm disk} < \tilde{\chi}^2_{\rm all}$, then the model was improved by the addition of a dust disk component. As noted above, this statistic can be large because it is dominated by a poor fit in the UV. It can also be large because the W3 (and/or W4) data points are bright compared to the model (see above, as well as individual target notes below); for example, removing the bright W3 and W4 points from the SED of WD 0420+520 reduces $\tilde{\chi}^2_{\rm disk}$ from 7.8 to 0.8.

Three targets-of-interest selected by our criteria (WD 1146-290, WD 1330+473, and WD 2152-548) show no strong IR excess (see Figure 3), and they are among the selected WDs with (W1−W2) color closest to the +0.3 mag criterion (see Figure 1). The first of these is a very cool WD (see Table 1 and notes below). It has a distinctive SED shape compared to the others in our selected sample, and its selection by our criteria was likely a by-product of its very low temperature. The latter two WDs have only very slightly elevated W2 flux densities compared to the WD model. In particular, *only* the W2 point in WD 2152-548 is elevated compared to the model; the adjacent IRAC-2 point (as well as the other IRAC data) agree with the model. Thus, the W2 value for WD 2152-548 should be treated with caution. If real, then the IR excesses in WD 1330+473 and WD 2152-548 are very weak and could indicate that only a small amount of cool dust is present. This situation presents similarities to the weak IR excesses found in PG 1457-086 (Farihi et al. 2009) and HE 0106-3253 (Farihi et al. 2010), which are inferred to be due to narrow circumstellar rings of dust instead of full disks, as well as to the several known WDs with combined gas and dust disks (e.g., Gänsicke et al. 2006; Brinkworth et al. 2009, 2012). The presence of co-mingled gas and dust disks could indicate that a significant amount of dust has been converted to gas through either sublimation (Melis et al. 2010) or collisions (with itself or possibly with pre-existing circumstellar material; Jura 2008; Girven et al. 2012).

2.1. Notes on Individual Targets

We have examined the publication record for each of the ten targets-of-interest, and briefly describe any relevant features below. We also vetted the *WISE* data for each of these sources for evidence of red contaminating sources in the photometry aperture (as described in Debes et al. 2011); relevant notes are included below.

2.1.1. WD 0249-052

Voss et al. (2007) and Limoges & Bergeron (2010) do not note any atmospheric contamination (including hydrogen) in this DB WD. In the former study, hydrogen was assumed to be absent unless a visual inspection of the optical spectrum revealed H lines (corresponding to a detection limit of Hα equivalent width $\gtrsim$ 300 mÅ). In the latter study, it appears that hydrogen was only utilized in the model spectrum analysis if the WD had been previously identified as a hydrogen-rich helium (DBA) WD. Additional examination of the two (somewhat noisy) spectra of this WD from the Voss et al. (2007) study yields no obvious metal lines, and limits of [Ca/He] < -8.0 and [Mg/He] < -6.7 (D. Koester, private communication). On the other hand, Bergeron et al. (2011) find [H/He]$= -5.47(59)$ (but no metals) by utilizing high S/N spectra of the Hα region. None of these three analyses, however, conclude that metal contamination (signified by the presence of Ca absorption in the optical spectrum) is present. We have no concerns about the quality of the *WISE* photometry.

2.1.2. WD 0420-731

There is no detailed information on this WD in the literature. However, there is a source (WISE-J041933.70-730333.9) located $\approx 22''$ northwest of the WD, which is faint in W1 and W2, but becomes much brighter in the W3 and W4 bands (slightly brighter than the WD). This source separation is well beyond the $1.3 \times (\mathrm{FWHM_{W1}}) \approx 7.8''$ radius, interior to which contamination of the *WISE* All Sky Catalog photometry can occur (see discussion in Debes et al. 2011); nonetheless, we tested for contamination from the neighboring source. To do so, we used the IRAF[7] implementation of DAOPHOT (Stetson 1987) to obtain PSF-fit photometry for the WD and the nearby source in the W3 Atlas images, using the nearby bright star WISE-J041948.50-730317.2 as a PSF template and magnitude calibrator. We obtain $\mathrm{W3_{psf}} = 11.69(40)$ mag for the WD and $\mathrm{W3_{psf}} = 11.60(33)$ mag for the nearby source, in agreement with the *WISE* catalog values of W3 $= 11.700(112)$ mag and W3 $= 11.642(106)$ mag, respectively. Nonetheless, the local background is patchy and bright in W3 and W4, so it is prudent to treat the W3 and W4 photometry as upper limits until higher

---

[7] IRAF is distributed by the National Optical Astronomy Observatories, which are operated by the Association of Universities for Research in Astronomy, Inc., under cooperative agreement with the National Science Foundation.

resolution imaging data are available.

2.1.3. WD 0420+520

There is no detailed information on this WD in the literature. The cataloged W3 and W4 flux densities for this target are quite bright, and there is no obvious point source at the position of the WD in the *WISE* W3 and W4 Atlas images. Thus, these values should be treated as upper limits.

2.1.4. WD 0836+404

This is a ZZ Ceti type pulsating WD (Vauclair et al. 1997). Farihi et al. (2005) found no evidence for a low luminosity companion from a survey utilizing proper motion measurements, deep imaging, and near-IR photometry. A limit on atmospheric metal contamination was set by Zuckerman et al. (2003), at [Ca/H]< -7.72.

There is a bright (V=10.9 mag) star (2MASS J08401164+4015211) located $\approx 43''$ east of the WD. While this star is far enough from the WD to not pose a contamination risk for the *WISE* photometry, we note that a diffraction spike from the star passes near the WD in the *WISE* Atlas images. Contamination warnings due to diffraction spikes are included in the *WISE* All Sky Catalog; such a warning was *not* flagged for WD 0836+404. Nonetheless, to confirm this we performed DAOPHOT PSF-subtraction photometry on the W2 Atlas image, as described above. We used the nearby stars WISE-J084000.92+401704.4 and WISE-J084022.86+401250.6 to construct a PSF template, and the mean photometry of the PSF stars plus several nearby stars (WISE-J083954.52+401509.5, WISE-J084001.71+401415.7, and WISE-J084022.35+401424.8) that are comparable in brightness to the WD as a magnitude calibrator. We obtain $W2_{psf} =$ 15.29(51) mag for the WD, in agreement with its *WISE* catalog value of W2= 15.245(115) mag. The nominal W2 PSF photometry for all 6 of the tested stars (including the WD) agrees to better than 1% with the *WISE* catalog values. So, we consider it unlikely that the nearby diffraction spike has contaminated the *WISE* photometry of the WD.

2.1.5. WD 1046-017

This is a known DB WD and there is tentative evidence that it might be metal-rich: Sion et al. (1988) noted a possible weak Ca II K feature in its optical spectrum (equivalent width < 10 mÅ), while Zuckerman et al. (2010), Bergeron et al. (2011), and Jura & Xu (2012) set limits of [Ca/He] < -10.9 (Ca II equivalent width $\lesssim 9$ mÅ), [H/He] $\lesssim -6.5$, and $\log(dM_{\mathrm{metals}}/dt$ [g s^{-1}]$) < 6.20$. Thus, the metal-rich status of this WD remains uncertain (but unlikely). Farihi et al. (2005) found no evidence for a low luminosity companion from a survey utilizing proper motion measurements,

deep imaging, and near-IR photometry. We have no concerns about the quality of the *WISE* photometry.

2.1.6. WD 1146-290

The equivalent width of Hα in this DA WD is 5.9 Å (Bergeron et al. 1997). There is no other detailed information on this WD in the literature. We have no concerns about the quality of the *WISE* photometry.

2.1.7. WD 1330+473

No IR excess or evidence for a dust disk is noted in the near- and mid-IR photometric and spectroscopic survey of Barber et al. (2012). Farihi et al. (2005) found no evidence for a low luminosity companion. We have no concerns about the quality of the *WISE* photometry.

2.1.8. WD 1448+411

There is no detailed information on this WD in the literature. We have no concerns about the quality of the *WISE* photometry.

2.1.9. WD 2152-548

This object was first discovered as an X-ray source in the *Einstein* satellite slew survey (Elvis et al. 1992), and was later confirmed as a hot DA WD optical counterpart to a *ROSAT* X-ray source (Mason et al. 1995; Marsh et al. 1997). Bannister et al. (2003) report possible weak photospheric metal contamination in this WD from high resolution UV spectroscopic observations, and note that it is "an object deserving of further attention." Dickinson et al. (2012) re-examined the origin of previously reported circumstellar features in 23 hot DA WDs. While unambiguous re-detections of circumstellar material were made for eight other WDs, they were unable to confirm the Ca II contamination reported by Bannister et al. (2003) for WD 2152-548. We have no concerns about the quality of the *WISE* photometry.

2.1.10. WD 2329+407

This WD was noted as non-magnetic in the spectropolarimetric survey of Schmidt & Smith (1995). Farihi et al. (2005) found no evidence for a low luminosity companion. There is a faint field

star located $\approx 8''$ southwest of the WD. Proper motion of the WD between the DSS-1 and -2 epochs shows that this object is not related to the WD. The neighboring source is visible in the 2MASS images but is not listed in the 2MASS Point Source Catalog. The W1 Atlas image shows a slight extension to the WD PSF that is consistent with the presence of this source, but is not visible in the W2 and W3 Atlas images (the WD is not visible at all in the W4 Atlas image; the W4 photometry for the WD is an upper limit). As with WD 0420-731, we performed DAOPHOT PSF-subtraction photometry, this time on the W1 Atlas image. We used the nearby bright star WISE-J233143.17+410133.1 as a PSF template, and the mean photometry of several nearby stars (WISE-J233140.08+410100.9, WISE-J233134.97+410217.7, WISE-J233129.20+410124.4, and WISE-J233135.68+410012.5) that are comparable in brightness to the WD as a magnitude calibrator. The corresponding PSF-subtraction of the WD was successful (see Figure 4), and we obtain $W1_{psf} = 13.75(5)$ mag, which is in agreement with the catalog photometry of W1= 13.757(27) mag. Thus, there appears to be no overt reason to be concerned about the *WISE* photometry of WD 2329+407.

3. Discussion and Conclusions

Many of the "original" WDs with dust disks that were discovered before 2011 have IR excesses that are detectable in the near-IR (JHK) bands. In all but one (WD 0420+520) of the new dust disk candidates presented here, the excess emission due to dust is only apparent at wavelengths $\gtrsim 3~\mu$m. It is possible that the current census of WDs with dust disks that produce an excess detectable at K-band and shorter wavelengths (e.g., using 2MASS or UKIDSS data; see Wachter et al. 2003; Wellhouse et al. 2005; Hoard et al. 2007; Steele et al. 2011) is close to complete for the entire sample of known WDs (at least to the detection limits of existing near-IR all-sky surveys). The WD dust disk candidates now being found using longer wavelength data from *WISE* and *Spitzer* are drawn from a previously underrepresented region of parameter space, in which the dust disks are overall cooler, narrower in radial extent, and/or contain fewer emitting grains.

In Figure 5, we have plotted the dust disk inner edge radius as a function of WD effective temperature for the seven new candidates from this paper, the candidates in Debes et al. (2011), and various published dust disk models for other WDs (see Table 5). There is a direct relationship between the WD temperature and the temperature of dust at a given radius (Jura 2003),

$$T_{\rm dust}(R) \propto R^{-3/4}\,T_{\rm wd}, \tag{1}$$

which is used to plot isotemperature contours in Figure 5 for the model dust disks. For an assumed dust sublimation temperature, the corresponding contour shows the minimum inner radius of the disk as a function of WD temperature; in general, the contours illustrate the temperature at a given radius in the disk for a given WD temperature. A typical boundary condition of WD dust disk models is that no dust is allowed to be hotter than the assumed sublimation temperature; in other words, dust is not allowed at radii closer to the WD than the radius at which the sublimation temperature (according to equation 1) is reached. In many cases, the hottest dust in the disk

models is at the assumed sublimation temperature (disk models with inner edges at the assumed sublimation temperature are indicated in Tables 4 and 5). Such a disk extends inward toward the WD as far as possible – its inner edge lies at the sublimation radius around the WD, so dust cannot survive any closer to the WD. On the other hand, disks that have inner edge radii corresponding to temperatures below the dust sublimation temperature could, in principle, extend inward closer to the WD but do not. In such cases, possible reasons for the lack of dust grains close to the WD include (but are not limited to):

- Grains close to the WD might have been depleted due to a higher rate of collisions with other grains. This might have occurred in the handful of known WDs with gas+dust disks, in which the gas and dust share spatially overlapping, but not identical, radial distributions, implying that dust sublimation alone cannot account for the presence of gas/lack of close-in dust (e.g., Brinkworth et al. 2012). Additionally, objects like WD 1456+298 (G166-158) have a very weak IR excess corresponding to the presence of only cool dust (see additional discussion of this object below).

- A spinning WD with a strong magnetic field might sweep up paramagnetic or diamagnetic dust grains interior to a critical radius. A similar process operates in the intermediate polar class of cataclysmic variable to produce a truncated gaseous accretion disk around the WD (see review of this class in Warner 2003). Based on observations of the Ca II lines during pulsations of the archetype dusty WD G29-38, Thompson et al. (2010) have suggested that the Ca is being accreted onto the poles of the WD, rather than equatorially, suggesting that the WD is magnetic. Brinkworth et al. (2007) (see the Appendix in that paper) calculated the critical surface charge on a dust grain, $Q_{\rm crit}$, such that the motion of the dust would be influenced by the WD magnetic field. They found that $Q_{\rm crit}$ for dust grains at the sublimation radius around a 14,200 K WD with a field strength of $B \approx 25$ MG is more than an order of magnitude larger than the likely surface charge of the grains based on observations of in situ interplanetary dust grains in the Solar System. However, they note that the value of $Q_{\rm crit}$ is several orders of magnitude smaller than the value $Q_{\rm max}$, at which the electrostatic tensile stress in the dust grain interiors would be sufficient to fracture (i.e., destroy) the grains. In addition, $Q_{\rm crit} \propto R^{3/2} B^{-1}$ (where R is the distance from the center of the WD to the dust grain), leaving open the possibility that magnetic interactions could be effective around WDs with larger magnetic fields and/or cooler temperatures (allowing the dust to approach closer to the WD before sublimating). Finally, Brinkworth et al. (2007) did not consider any intrinsic para- or diamagnetic properties of the dust itself, which could enhance interaction with the WD magnetic field. Other than these two examples (one observational, one theoretical), there has been (to our knowledge) little exploration of this possibility.

There is, of course, some ambiguity in the interpretation of Figure 5. A given disk could appear to not reach the sublimation radius if the assumed sublimation temperature was higher than the true sublimation temperature for the particular species of dust in the observed disk. In the bulk of

cases, however, the published models of dust disks extend inward to the sublimation radius even when the assumed sublimation temperature is quite high (e.g., a majority of the large sample in Debes et al. 2011 with $T_{\rm subl} = 2100$ K, or WD 0420+520 in this work). Apparently, most of the currently known dusty WDs have "hot" disks in which the dust extends inward quite close to the WD, until it reaches the "sublimation barrier." In contrast, five of the seven dust disk candidates presented here have maximum dust temperatures of $\lesssim 1000$ K, safely below reasonable lower limits of the sublimation temperature for metallic dust. They are, therefore, truly "cool" disks in which dust is depleted close to the WD and is mainly present substantially exterior to the sublimation radius. These disks are narrower in radial extent than an otherwise identical disk in which the inner edge extends all the way to the sublimation radius. The apparent bias toward sublimation-limited disks does not, however, imply that "hot" WD dust disks are necessarily more intrinsically common than "cool" disks. The "hot" disks are easier to find, since they produce strong IR excesses that can be detected in the near-IR.

Three of our dust disk candidates (WD 0249-052, WD 0836+404, WD 1046-017) have published optical spectroscopic studies noting the absence of atmospheric metal pollution. One would expect to find metals in the atmosphere of a WD with an IR excess indicating a dust disk, as some of the dust will accrete onto the star. The DB WDs (WD 0249-052, WD 1046-017) have gravitational settling times for metals in their helium-rich atmospheres that are much longer than for DA WDs; metals can persist for up to a Myr or longer after accretion ceases, making them appear as metal-rich WDs for a substantial time after the dust disk has dissipated (typical disk lifetimes are ∼0.03–5 Myr; Girven et al. 2012). While there appear to be firm constraints on the lack of accreted metals in WD 0249-052 (see Section 2.1.1), the situation for WD 1046-017 is less certain (see Section 2.1.5). Possibly the most viable explanation for the presence of a dust disk around a DB WD that is not metal-polluted is that the disk is newly formed and the abundance of accreted metals on the WD is not yet in a steady state and has not reached the threshold of detection.

On the other hand, because of the short settling times of DA WDs, essentially any process that causes the accretion of metals from the dust disk to be out of steady state could produce the phenomenon of a WD with an IR excess but no spectroscopic signature of metal pollution. In the case of the DA WD among these three, we note that the limit on the metal contamination of WD 0836+404 is not very stringent ([Ca/H]< -7.7; Zuckerman et al. 2003). This leaves some ambiguity in the conclusion that the WD has no metal pollution; for example, the SED of WD 0836+404 (like the other two; also see discussion above) is similar in appearance to that of G166-158. The latter is a metal-polluted DA WD with a very weak IR excess that only becomes apparent longward of ≈ 5 μm, and likely indicates a narrow annulus of cool dust located relatively far from the WD with a large, inner, dust-free zone. Zuckerman et al. (2003) measured [Ca/H]$= -9.3$ for G166-158, implying that WD 0836+404 could still be considered metal-rich with [Ca/H]< -7.7, even if the true Ca abundance limit is an order of magnitude lower, given that Zuckerman et al. (2003) assumed a somewhat higher temperature for WD 0836+404. By the same token, WD 0836+404 (~ 11700 K) is hotter than G166-158 (~ 7400 K), so the former would require

a higher Ca abundance to show lines than the latter (i.e., they could have comparable levels of Ca enrichment, but only the cooler WD might show Ca lines in its optical spectrum). Regardless, a DA WD with a dust disk but no metal pollution might be explained by a number of scenarios, including the inner disk dust depletion and "magnetic sweeping" scenarios discussed above, as well as non-steady state accretion from a newly-formed dust disk (as suggested above for the case of DB WDs).

We end with a final note of caution. As discussed in Debes et al. (2011), the large *WISE* PSF can defy even the most careful vetting process and allow unidentified contamination from faint, red, unresolved sources. Thus, the seven WDs highlighted here should be considered only as dust disk *candidates* until independent confirmation of their IR excesses can be obtained. This is especially true for the three WDs, discussed above, that do not appear to show the signature of metal contamination in their optical spectra. In these cases, the existing IR data do not strongly constrain a dust disk model. Additional longer wavelength mid-IR observations are needed to rule out the possibility that a very cool brown dwarf companion could be responsible for the observed IR excess.

Johns Hopkins University, the Joint Institute for Nuclear Astrophysics, the Kavli Institute for Particle Astrophysics and Cosmology, the Korean Scientist Group, the Chinese Academy of Sciences (LAMOST), Los Alamos National Laboratory, the Max-Planck-Institute for Astronomy (MPIA), the Max-Planck-Institute for Astrophysics (MPA), New Mexico State University, Ohio State University, University of Pittsburgh, University of Portsmouth, Princeton University, the United States Naval Observatory, and the University of Washington. (h) The *Wide-field Infrared Survey Explorer* (*WISE*), which is a joint project of the University of California, Los Angeles, and JPL, Caltech, funded by NASA.

Facilities: 2MASS, AAVSO, GALEX, SDSS, Spitzer (IRAC, MIPS), WISE

REFERENCES

Abazajian, K. N., Adelman-McCarthy, J. K., Agüeros, M. A., et al. 2009, ApJS, 182, 543

Antonucci, R. 1993, ARA&A, 31, 473

Aumann, H. H. 1985, PASP, 97, 885

Bannister, N. P., Barstow, M. A., Holberg, J. B., & Bruhweiler, F. C. 2003, MNRAS, 341, 477

Barber, S. D., Patterson, A. J., Kilic, M., et al. 2012, ApJ, 760, 26

Barstow, M. A., Bond, H. E., Burleigh, M. R., & Holberg, J. B. 2001, MNRAS, 322, 891

Barstow, M. A., Holberg, J. B., Fleming, T. A., et al. 1994, MNRAS, 270, 499

Becklin, E. E., Farihi, J., Jura, M., et al. 2005, ApJ, 632, L119

Bergeron, P., Ruiz, M. T., & Leggett, S. K. 1997, ApJS, 108, 339

Bergeron, P., Wesemael, F., & Beauchamp, A. 1995, PASP, 107, 1047

Bergeron, P., Wesemael, F., Dufour, P., et al. 2011, ApJ, 737, 28

Bessell, M. S. 1979, PASP, 91, 589

Bradley, P. A. 2000, Baltic Astronomy, 9, 485

Brinkworth, C. S., Gänsicke, B. T., Girven, J. M., et al. 2012, ApJ, 750, 86

Brinkworth, C. S., Gänsicke, B. T., Marsh, T. R., Hoard, D. W., & Tappert, C. 2009, ApJ, 696, 1402

Brinkworth, C. S., Hoard, D. W., Wachter, S., et al. 2007, ApJ, 659, 1541

Chini, R., Kruegel, E., Kreysa, E., Shustov, B., & Tutukov, A. 1991, A&A, 252, 220

Chu, Y.-H., Gruendl, R. A., Guerrero, M. A., et al. 2009, AJ, 138, 691

Debes, J. H., Hoard, D. W., Kilic, M., et al. 2011, ApJ, 729, 4

Debes, J. H., Hoard, D. W., Wachter, S., Leisawitz, D. T., & Cohen, M. 2011, ApJS, 197, 38

Debes, J. H., & Sigurdsson, S. 2002, ApJ, 572, 556

Debes, J. H., Walsh, K. J., & Stark, C. 2012, ApJ, 747, 148

Dickinson, N. J., Barstow, M. A., Welsh, B. Y., et al. 2012, MNRAS, 423, 1397

Elvis, M., Plummer, D., Schachter, J., & Fabbiano, G. 1992, ApJS, 80, 257

Farihi, J. 2011, White Dwarf Atmospheres and Circumstellar Environments, ed. D. W. Hoard (Berlin: Wiley VCH), 117

Farihi, J., Barstow, M. A., Redfield, S., Dufour, P., & Hambly, N. C. 2010, MNRAS, 404, 2123

Farihi, J., Becklin, E. E., & Zuckerman, B. 2005, ApJS, 161, 394

Farihi, J., Brinkworth, C. S., Gänsicke, B. T., et al. 2011, ApJ, 728, L8

Farihi, J., Gänsicke, B. T., Steele, P. R., et al. 2012, MNRAS, 421, 1635

Farihi, J., Jura, M., Lee, J.-E., & Zuckerman, B. 2010, ApJ, 714, 1386

Farihi, J., Jura, M., & Zuckerman, B. 2009, ApJ, 694, 805

Farihi, J., Zuckerman, B., & Becklin, E. E. 2008, ApJ, 674, 431

Fleming, T. A., Green, R. F., Jannuzi, B. T., et al. 1993, AJ, 106, 1729

Fleming, T. A., Schmitt, J. H. M. M., Barstow, M. A., & Mittaz, J. P. D. 1991, A&A, 246, L47

Gänsicke, B. T., Marsh, T. R., Southworth, J., & Rebassa-Mansergas, A. 2006, Science, 314, 1908

Gänsicke, B. T., Koester, D., Farihi, J., Girven, J., Parsons, S. G., & Breedt, E. 2012, MNRAS, 424, 333

Gianninas, A., Bergeron, P., Dupuis, J., & Ruiz, M. T. 2010, ApJ, 720, 581

Girven, J., Brinkworth, C. S., Farihi, J., et al. 2012, ApJ, 749, 154

Griffin, R. F., & Keenan, P. C. 1992, The Observatory, 112, 168

Henize, K. G., & Fairall, A. P. 1981, PASP, 93, 435

Hoard, D. W., Wachter, S., Sturch, L. K., et al. 2007, AJ, 134, 26

Holberg, J. B., & Bergeron, P. 2006, AJ, 132, 1221

Jura, M. 2003, ApJ, 584, L91

Jura, M. 2008, AJ, 135, 1785

Jura, M., Farihi, J., & Zuckerman, B. 2007a, ApJ, 663, 1285

Jura, M., Farihi, J., Zuckerman, B., & Becklin, E. E. 2007b, AJ, 133, 1927

Jura, M., Farihi, J., & Zuckerman, B. 2009, AJ, 137, 3191

Jura, M., & Xu, S. 2012, AJ, 143, 6

Kilic, M., Patterson, A. J., Barber, S., Leggett, S. K., & Dufour, P. 2012, MNRAS, 419, L59

Kilic, M., & Redfield, S. 2007, ApJ, 660, 641

Kilic, M., von Hippel, T., Leggett, S. K., & Winget, D. E. 2005, ApJ, 632, L115

Kilic, M., von Hippel, T., Leggett, S. K., & Winget, D. E. 2006, ApJ, 646, 474

Kobayashi, H., Kimura, H., Watanabe, S.-i., Yamamoto, T., & Müller, S. 2011, Earth, Planets, and Space, 63, 1067

Koester, D., Provencal, J., & Shipman, H. L. 1997, A&A, 320, L57

Koester, D., Voss, B., Napiwotzki, R., et al. 2009, A&A, 505, 441

Kuchner, M. J., Koresko, C. D., & Brown, M. E. 1998, ApJ, 508, L81

Kwitter, K. B., & Jacoby, G. H. 1989, AJ, 98, 2159

Lacombe, P., Wesemael, F., Fontaine, G., & Liebert, J. 1983, ApJ, 272, 660

Liebert, J., Bergeron, P., & Holberg, J. B. 2005, ApJS, 156, 47

Liebert, J., Green, R., Bond, H. E., et al. 1989, ApJ, 346, 251

Limoges, M.-M., & Bergeron, P. 2010, ApJ, 714, 1037

Marsh, M. C., Barstow, M. A., Buckley, D. A., et al. 1997, MNRAS, 287, 705

Martin, D. C., Fanson, J., Schiminovich, D., et al. 2005, ApJ, 619, L1

Mason, K. O., Hassall, B. J. M., Bromage, G. E., et al. 1995, MNRAS, 274, 1194

McCook, G. P., & Sion, E. M. 1999, ApJS, 121, 1

Melis, C., Farihi, J., Dufour, P., et al. 2011, ApJ, 732, 90

Melis, C., Jura, M., Albert, L., Klein, B., & Zuckerman, B. 2010, ApJ, 722, 1078

Mullally, F., Kilic, M., Reach, W. T., et al. 2007, ApJS, 171, 206

Napiwotzki, R. 1993, Acta Astron., 43, 343

Napiwotzki, R., & Schoenberner, D. 1995, A&A, 301, 545

Natta, A. 2008, Physica Scripta Volume T, 130, 014014

Nuth, J. A., III, & Hecht, J. H. 1990, Ap&SS, 163, 79

Papoular, R., & Pegourie, B. 1983, A&A, 128, 335

Pollack, J. B., Hollenbach, D., Beckwith, S., Simonelli, D. P., Roush, T., & Fong, W. 1994, ApJ, 421, 615

Rafikov, R. R., & Garmilla, J. A. 2012, ApJ, 760, 123

Rauch, T., Koeppen, J., & Werner, K. 1994, A&A, 286, 543

Rauch, T., & Werner, K. 1993, Astronomische Gesellschaft Abstract Series, 9, 155

Rauch, T., & Werner, K. 1995, White Dwarfs, 443, 186

Reach, W. T., Lisse, C., von Hippel, T., & Mullally, F. 2009, ApJ, 693, 697

Rowan-Robinson, M. 1977, ApJ, 213, 635

Schindler, M., Linsky, J. L., Helfand, D. J., Stencel, R. E., & Basri, G. S. 1982, ApJ, 263, 269

Schmidt, G. D., & Smith, P. S. 1995, ApJ, 448, 305

Schoenberner, D., & Napiwotzki, R. 1990, A&A, 231, L33

Shara, M. M., Bergeron, I. E., Christian, C. A., Craig, N., & Bowyer, S. 1997, PASP, 109, 998

Shipman, H. L., & Greenstein, J. L. 1983, ApJ, 266, 761

Sion, E. M., Aannestad, P. A., & Kenyon, S. J. 1988, ApJ, 330, L55

Sion, E. M., Fritz, M. L., McMullin, J. P., & Lallo, M. D. 1988, AJ, 96, 251

Sion, E. M., Kenyon, S. J., & Aannestad, P. A. 1990, ApJS, 72, 707

Skrutskie, M. F., Cutri, R. M., Stiening, R., et al. 2006, AJ, 131, 1163

Starrfield, S., Cox, A. N., Kidman, R. B., & Pensnell, W. D. 1985, ApJ, 293, L23

Steele, P. R., Burleigh, M. R., Dobbie, P. D., et al. 2011, MNRAS, 416, 2768

Stetson, P. B. 1987, PASP, 99, 191

Suh, K.-W. 1999, MNRAS, 304, 389

Thompson, S. P., Fonti, S., Verrienti, C., et al. 2003, Meteoritics and Planetary Science, 38, 457

Thompson, S. E., Montgomery, M. H., von Hippel, T., et al. 2010, ApJ, 714, 296

Vauclair, G., Dolez, N., Fu, J. N., & Chevreton, M. 1997, A&A, 322, 155

Verbiscer, A. J., Skrutskie, M. F., & Hamilton, D. P. 2009, Nature, 461, 1098

von Hippel, T., Kuchner, M. J., Kilic, M., Mullally, F., & Reach, W. T. 2007, ApJ, 662, 544

Voss, B., Koester, D., Napiwotzki, R., Christlieb, N., & Reimers, D. 2007, A&A, 470, 1079

Wachter, S., Hoard, D. W., Hansen, K. H., et al. 2003, ApJ, 586, 1356

Warner, B. 2003, Cataclysmic Variable Stars (Cambridge, UK: Cambridge University Press)

Wellhouse, J. W., Hoard, D. W., Howell, S. B., Wachter, S., & Esin, A. A. 2005, PASP, 117, 1378

Wright, E. L., Eisenhardt, P. R. M., Mainzer, A. K., et al. 2010, AJ, 140, 1868

Xu, S., & Jura, M. 2012, ApJ, 745, 88

Xu, D. W., Wei, J. Y., Dong, X. Y., & Hu, J. Y. 1999, A&AS, 134, 365

Zeidler-K.T., E.-M., Weidemann, V., & Koester, D. 1986, A&A, 155, 356

Zuckerman, B., & Becklin, E. E. 1987, Nature, 330, 138

Zuckerman, B., Koester, D., Dufour, P., et al. 2011, ApJ, 739, 101

Zuckerman, B., Koester, D., Melis, C., Hansen, B. M., & Jura, M. 2007, ApJ, 671, 872

Zuckerman, B., Koester, D., Reid, I. N., & Hünsch, M. 2003, ApJ, 596, 477

Zuckerman, B., Melis, C., Klein, B., Koester, D., & Jura, M. 2010, ApJ, 722, 725
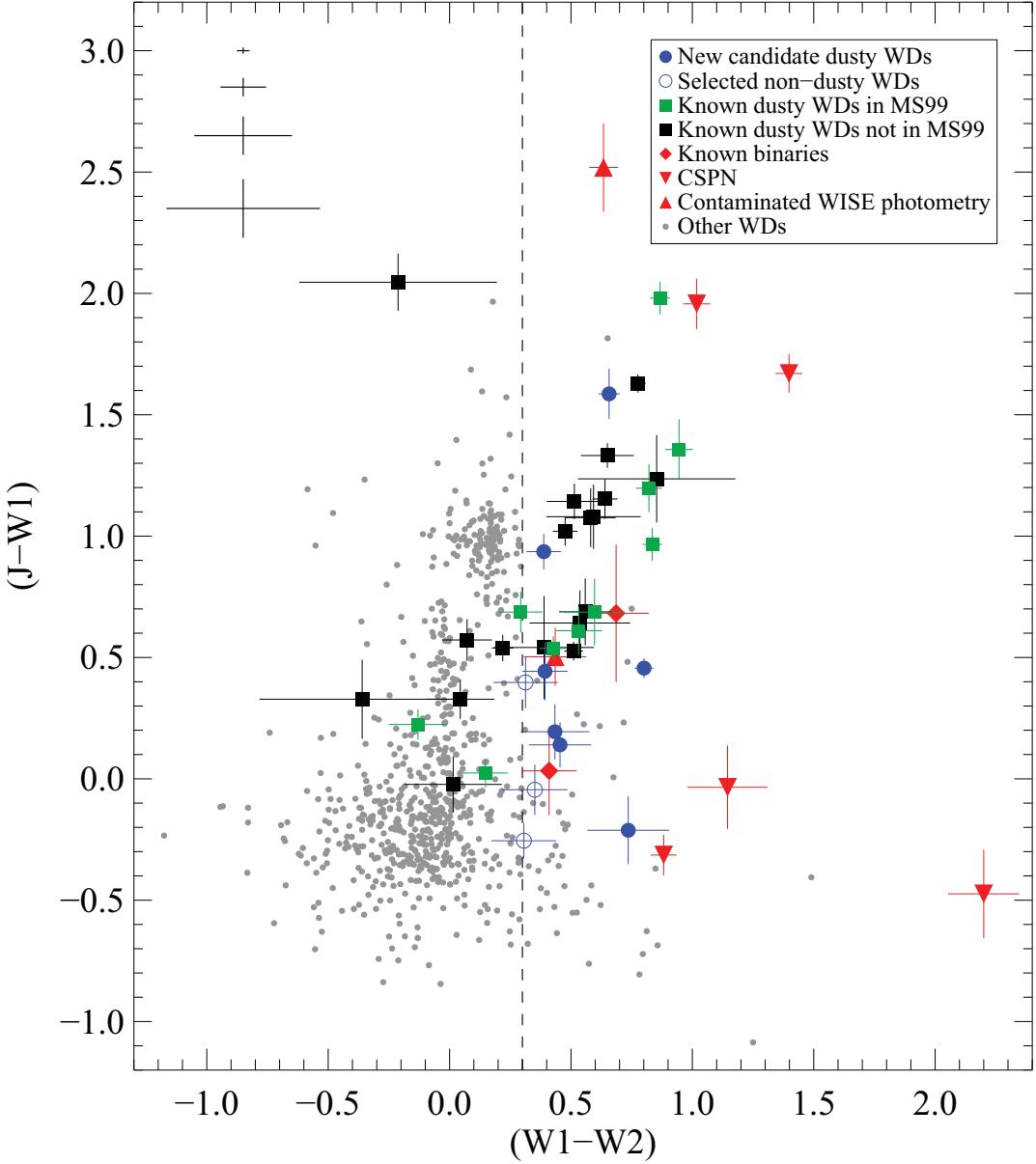
Fig. 1.— Infrared color-color diagram of MS99 WDs with 2MASS J and *WISE* W1 and W2 detections. The vertical dashed line marks a (W1−W2) color of +0.3 mag, which was used in the target selection process. Representative color index error bars are shown in the upper left; from top to bottom, 25%, 50%, 75%, and 90% of the detected targets have photometric uncertainties smaller than the indicated error bars. The points are symbol-coded as follows: new candidate WDs with dust disks (blue filled circles), selected targets that are not dust disk candidates (blue unfilled circles), known WDs with dust disks that are in (green squares) or not in (black squares) MS99, known unresolved binaries (red diamonds), central stars of planetary nebulae (red downward facing triangles), *WISE* photometry is contaminated (red upward facing triangles), and remaining WDs that did not satisfy our selection criteria as targets-of-interest (small gray circles). WD 1201+437 is also a known unresolved binary with (J−W1) = +3.8 mag and, for clarity, is the only target not plotted here.
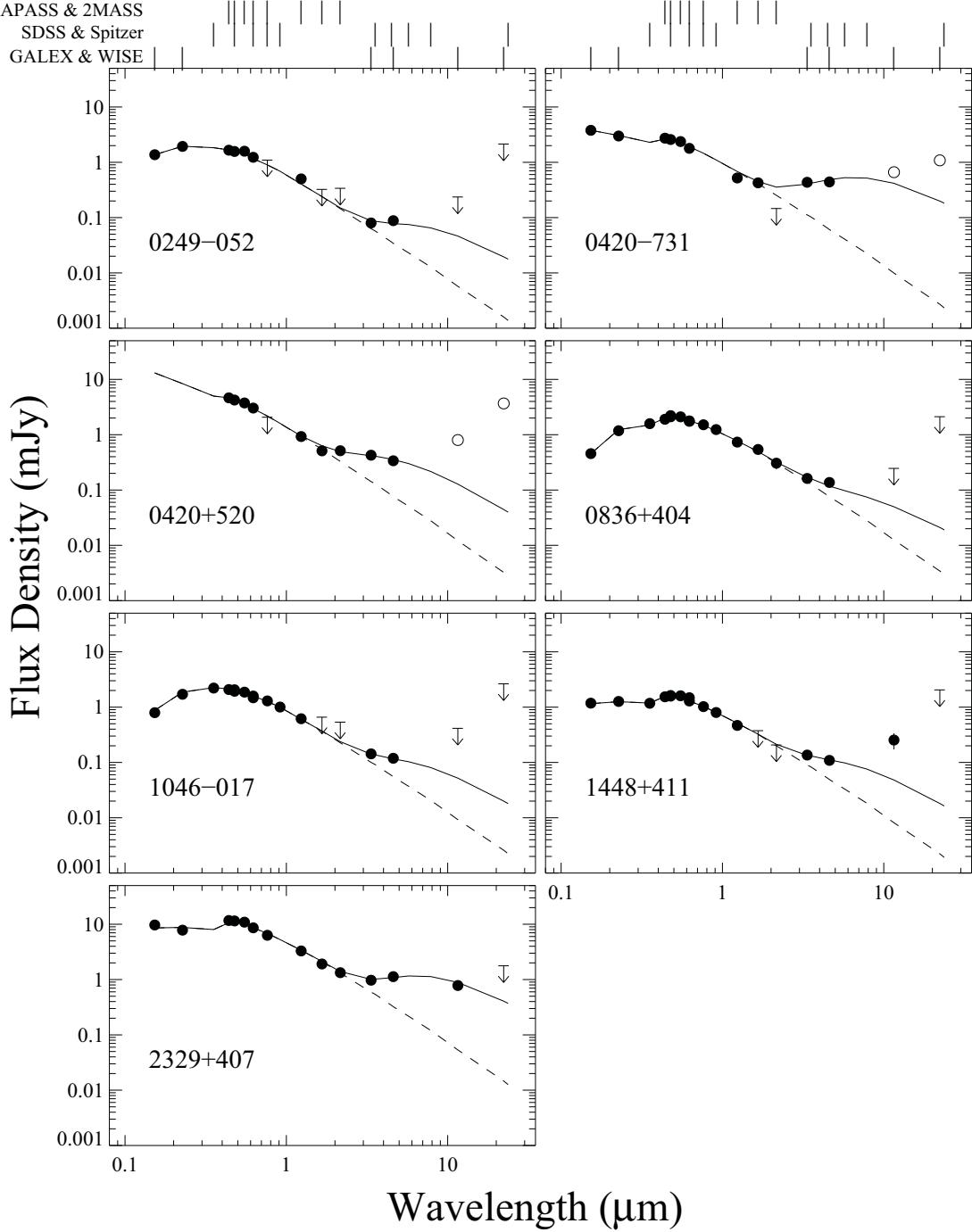
Fig. 2.— Spectral energy distributions of the seven new WD with dust disk candidates. Photometric values are shown as filled circles; cataloged 2σ (95% confidence) upper limits for non-detections are shown as downward arrows. The unfilled circles are W3 and W4 photometry that is of questionable quality and should be treated as upper limits (see Sections 2.1.2 and 2.1.3). The wavelengths of the various photometric bands are indicated at the top of the figure (see Tables 1–3 for the wavelength of each band). The dashed line is a WD model fit, while the solid line is a combined WD + dust disk model (see Table 4 for disk parameters). The two models are generally indistinguishable shortward of ≈ 2 μm.
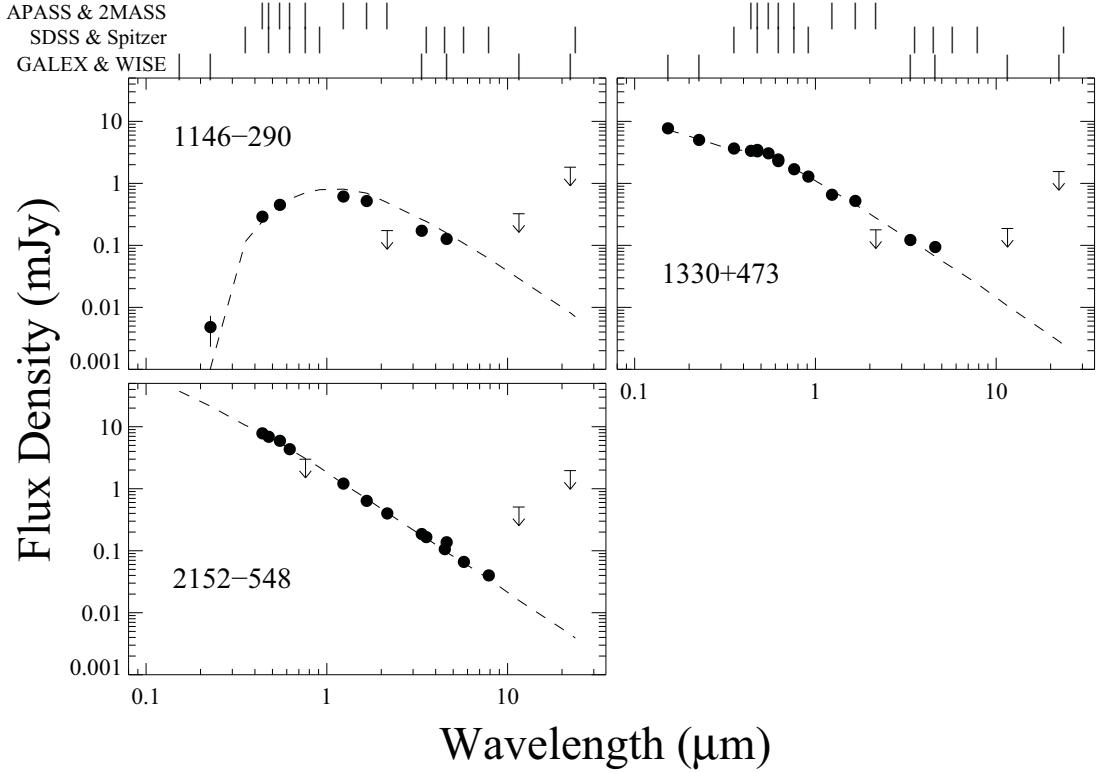
Fig. 3.— As in Figure 2, but for the three WDs selected by our target criteria that are not dust disk candidates.
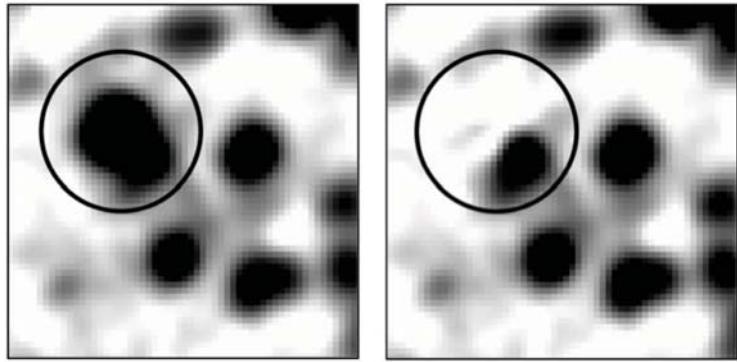
Fig. 4.— The *WISE* W1 Atlas image of WD 2329+407 before (left panel) and after (right panel) PSF-subtraction of the WD. The circle is centered on the WD and shows the extent of the PSF radial profile fit. The image is $\approx 80''$ in both dimensions, with a plate scale of $\approx 1.4''$ pixel^{-1}, and is oriented north up, west to the right. This figure is representative of all of the PSF subtraction photometry performed here, as discussed in Section 2.1.
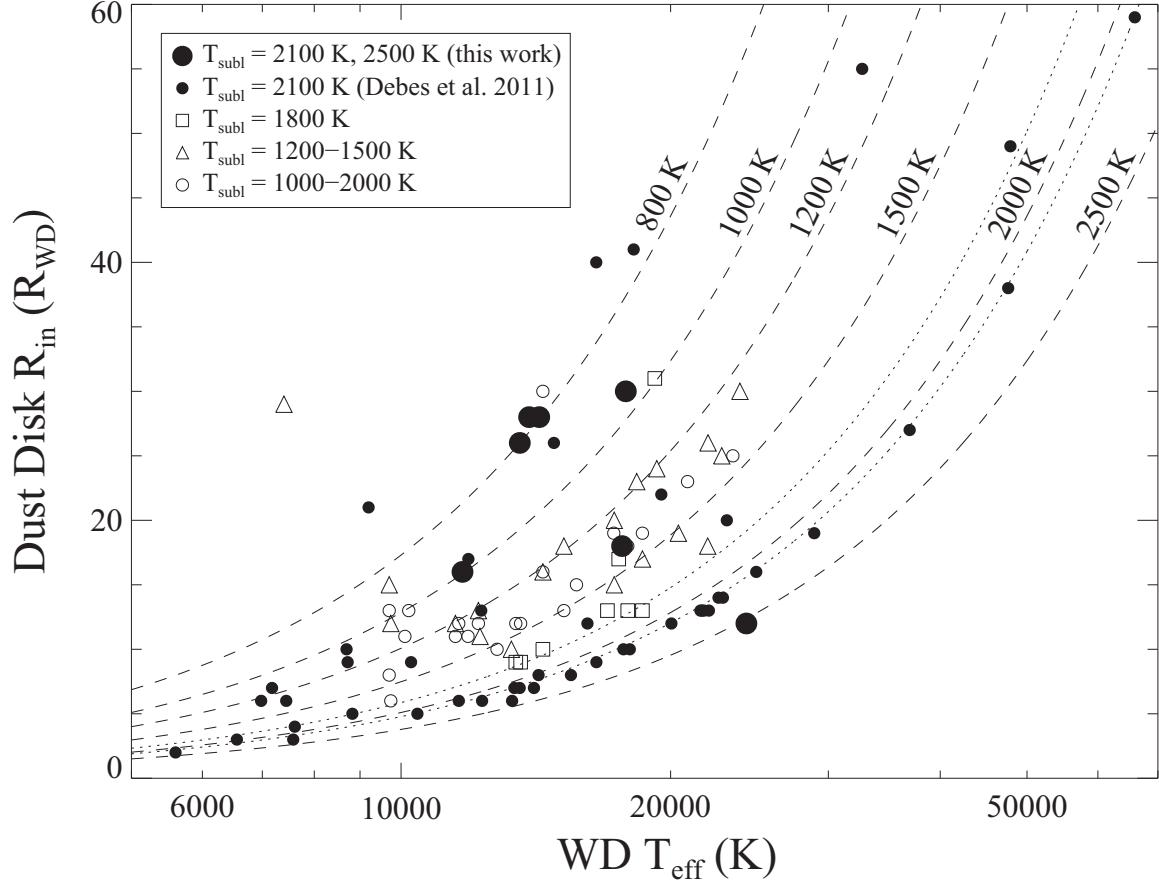
Fig. 5.— Inner edge radius as a function of WD effective temperature for published WD dust disk models. The dashed lines are isotemperature contours that show the temperature at a given radius in the disk for a given WD temperature. Models that are "sublimation-limited" (i.e., the dust located closest to the WD is constrained to be no hotter than the sublimation temperature) will lie along the isotemperature contour corresponding to the dust sublimation temperature assumed in the model. The small filled circles are the new WD dust disk candidates from Debes et al. (2011) (with assumed sublimation temperature of 2100 K, shown as a dotted isotemperature contour) and the large filled circles are the new candidates from this work. The other points are previously known WD dust disks, using published disk models and WD effective temperatures (see Table 5; some WDs are plotted more than once corresponding to different published dust disk model parameters), and are symbol-coded as follows: unfilled triangles represent models with assumed sublimation temperatures of 1200–1500 K, unfilled squares have assumed sublimation temperature of 1800 K (shown as a dotted isotemperature contour), and unfilled circles have various assumed sublimation temperatures in the range 1000–2000 K. Disk radii were rounded to integers, so some plotted points fall at radius values slightly smaller or larger than the minimum radius for the corresponding assumed sublimation temperature. See text for additional discussion.

Table 1. System Parameters and Photometry (UV, near-IR) of Selected MS99 White Dwarfs

WD	WISE Designation	Type[a]	$T_{\rm eff}$ (K)	log g	Refs	GALEX: fuv (mag) (μJy) [0.1528 μm]	nuv (mag) (μJy) [0.2271 μm]	2MASS: J (mag) (μJy) [1.235 μm]	H (mag) (μJy) [1.662 μm]	Ks (mag) (μJy) [2.159 μm]
New WD Dust Disk Candidates:										
0249–052	J025215.53-050231.3	DB	17700 ± 548	8.16 ± 0.09	1	16.057 ± 0.033 1371 ± 42	15.682 ± 0.016 1937 ± 28	16.256 ± 0.116 501^{+52}_{-57}	>16.249 <324	>15.735 <339
0420–731	J041937.81-730344.3	DA	...	...	2	14.955 ± 0.019 3783 ± 67	15.212 ± 0.015 2987 ± 40	16.217 ± 0.099 520^{+46}_{-50}	15.954 ± 0.179 425^{+65}_{-77}	>16.646 <146
0420+520	J042415.70+521010.6	DA	26142 ± 3921	8.1	3	... ...	... ...	15.589 ± 0.062 927^{+54}_{-57}	15.755 ± 0.172 511^{+76}_{-88}	15.284 ± 0.156 513^{+69}_{-80}
0836+404	J084007.64+401503.6	DA	11870 ± 180	8.10 ± 0.05	4	17.254 ± 0.048 455 ± 20	16.219 ± 0.020 1181 ± 22	15.840 ± 0.073 735^{+50}_{-53}	15.693 ± 0.130 541^{+62}_{-70}	15.845 ± 0.219 306^{+56}_{-69}
1046–017	J104832.65-020112.3	DB(Z?)	14620 ± 354	8.14 ± 0.13	1	16.651 ± 0.039 794 ± 28	15.819 ± 0.009 1708 ± 13	16.030 ± 0.089 617^{+50}_{-54}	>15.481 <658	>15.240 <535
1448+411	J145006.54+405533.7	DA	...	...	2	16.221 ± 0.031 1180 ± 34	16.143 ± 0.019 1267 ± 22	16.333 ± 0.111 467^{+46}_{-51}	>16.092 <375	>16.271 <207
2329+407	J233135.90+410129.6	DA	15900	7.91	5	13.933 ± 0.008 9698 ± 71	14.167 ± 0.006 7816 ± 43	14.213 ± 0.031 3291^{+109}_{-111}	14.322 ± 0.058 1912^{+106}_{-111}	14.249 ± 0.070 1332^{+87}_{-92}
Other Selected WDs:										
1146–290	J114904.63-292150.8	DA	5770 ± 140	8.00	6	... ...	22.195 ± 0.560 5 ± 3	16.037 ± 0.092 613^{+51}_{-55}	15.737 ± 0.172 519^{+77}_{-90}	>16.462 <173
1330+473	J133236.00+470411.0	DA	22570	7.89	5	14.181 ± 0.001 7722 ± 8	14.649 ± 0.001 5018 ± 3	15.966 ± 0.086 655^{+51}_{-55}	15.734 ± 0.155 521^{+70}_{-81}	>16.434 <178
2152–548	J215621.35-543823.3	DA	45171 ± 121	7.878 ± 0.009	7	... ...	... ...	15.300 ± 0.047 1209^{+55}_{-57}	15.515 ± 0.116 637^{+66}_{-73}	15.554 ± 0.194 400^{+66}_{-79}

Table 1—Continued

WD	WISE Designation	Type[a]	T_{eff} (K)	log g	Refs	GALEX: fuv (mag) (μJy) [0.1528 μm]	nuv (mag) (μJy) [0.2271 μm]	2MASS: J (mag) (μJy) [1.235 μm]	H (mag) (μJy) [1.662 μm]	Ks (mag) (μJy) [2.159 μm]
EXCLUDED – Known WDs with Dust Disks:										
0408-041	J041102.16-035823.7	DAZ	15414 ± 45	7.856 ± 0.010	7	15.580 ± 0.018 / 2128 ± 35	15.592 ± 0.012 / 2105 ± 22	15.870 ± 0.061 / 715^{+41}_{-43}	15.991 ± 0.129 / 411^{+47}_{-52}	15.440 ± 0.175 / 445^{+67}_{-78}
0843+516	J084702.27+512852.6	DA	23876	7.9	5	15.132 ± 0.018 / 3214 ± 55	15.394 ± 0.002 / 2527 ± 5	16.585 ± 0.123 / 370^{+40}_{-45}	16.481 ± 0.232 / 262^{+51}_{-63}	>16.543 / <161
1015-161	J101803.75+155158.1	DAZ	19948 ± 33	7.925 ± 0.006	7	14.991 ± 0.013 / 3661 ± 44	15.213 ± 0.006 / 2983 ± 17	16.131 ± 0.085 / 562^{+43}_{-47}	16.120 ± 0.222 / 365^{+68}_{-83}	16.003 ± 0.216 / 265^{+48}_{-58}
1116+026	J111912.32+022033.9	DA	12121 ± 23	8.005 ± 0.005	7	15.666 ± 0.007 / 1966 ± 12	15.078 ± 0.002 / 3380 ± 7	14.752 ± 0.039 / 2003^{+79}_{-81}	14.730 ± 0.051 / 1313^{+65}_{-68}	14.611 ± 0.105 / 954^{+90}_{-99}
1150-153	J115315.23-153637.0	DAZ	12132(42)	8.033 ± 0.008	7	17.332 ± 0.056 / 424 ± 22	16.524 ± 0.024 / 892 ± 20	16.038 ± 0.119 / 613^{+64}_{-71}	15.926 ± 0.173 / 436^{+65}_{-76}	>16.119 / <238
1541+650	J154144.90+645352.3	DA	11600 ± 178	8.10 ± 0.05	8	17.002 ± 0.048 / 574 ± 25	16.090 ± 0.021 / 1330 ± 26	15.604 ± 0.062 / 914^{+53}_{-56}	15.912 ± 0.171 / 442^{+65}_{-76}	15.429 ± 0.175 / 449^{+67}_{-79}
1729+371	J173134.34+370518.5	DAZ	10540 ± 200	8.24 ± 0.04	9	20.782 ± 0.227 / 18 ± 4	17.257 ± 0.028 / 454 ± 12	16.162 ± 0.093 / 547^{+46}_{-50}	>16.070 / <382	>15.604 / <382
EXCLUDED – WD is a CSPN (central star of a planetary nebula):										
0558-756	J055702.22-754020.7	DO	100000 ± 15000	6.5 ± 0.5	10	14.107 ± 0.012 / 8266 ± 88	14.573 ± 0.009 / 5381 ± 46	16.403 ± 0.120 / 438^{+46}_{-52}	>16.490 / <260	>15.818 / <314
0950+139	J095258.96+134434.7	DA	93230	7.36	11	13.720 ± 0.001 / 11807 ± 15	14.777 ± 0.002 / 4458 ± 6	16.518 ± 0.097 / 394^{+34}_{-37}	15.945 ± 0.157 / 429^{+58}_{-67}	16.099 ± 0.258 / 242^{+51}_{-65}
1821+643	J182152.09+642153.7	DOZ	140000	6.1	12,13	12.669 ± 0.001 / 31086 ± 21	13.292 ± 0.001 / 17502 ± 11	15.784 ± 0.076 / 774^{+54}_{-58}	15.996 ± 0.190 / 409^{+66}_{-79}	>15.468 / <433

Table 1—Continued

WD	WISE Designation	Type[a]	$T_{\rm eff}$ (K)	$\log g$	Refs	GALEX: fuv (mag) (μJy) [0.1528 μm]	nuv (mag) (μJy) [0.2271 μm]	2MASS: J (mag) (μJy) [1.235 μm]	H (mag) (μJy) [1.662 μm]	Ks (mag) (μJy) [2.159 μm]
1958+015	J200039.34+014341.6	PG1159	58900	$\cdots$	14	14.688 ± 0.008 4840 ± 37	15.286 ± 0.005 2789 ± 14	15.428 ± 0.065 1075^{+65}_{-69}	14.830 ± 0.074 1198^{+82}_{-88}	14.603 ± 0.106 961^{+91}_{-100}
2333+301	J233553.29+302805.6	DOZ	150000	7.0	15,16	$\cdots$ $\cdots$	14.603 ± 0.002 5235 ± 10	16.697 ± 0.136 334^{+40}_{-45}	> 16.995 < 163	> 17.164 < 91

[a]From MS99 and MSonline.

Note. — Upper limits are 2σ (95% confidence) levels. References: (1) Bergeron et al. (2011), (2) no published $T_{\rm eff}$ or $\log g$ values, (3) Sion et al. (1988), (4) Limoges & Bergeron (2010), (5) Holberg & Bergeron (2006), (6) Bergeron et al. (1997), (7) Koester et al. (2009), (8) Liebert et al. (2005), (9) Zuckerman et al. (2007), (10) Rauch et al. (1994), (11) Gianninas et al. (2010), (12) Bradley (2000), (13) Rauch & Werner (1995), (14) Kwitter & Jacoby (1989), (15) Chu et al. (2009), (16) Napiwotzki (1993)

Table 2. Optical Photometry of Selected MS99 White Dwarfs

WD	SDSS: u (mag) (μJy) [0.3543 μm]	g (mag) (μJy) [0.4770 μm]	r (mag) (μJy) [0.6231 μm]	i (mag) (μJy) [0.7625 μm]	z (mag) (μJy) [0.9134 μm]	APASS: B (mag) (μJy) [0.44 μm]	V (mag) (μJy) [0.55 μm]	g (mag) (μJy) [0.4770 μm]	r (mag) (μJy) [0.6231 μm]	i (mag) (μJy) [0.7625 μm]
New WD Dust Disk Candidates:										
0249-052	...	...	...	...	...	15.993 ± 0.006 1655 ± 51	15.943 ± 0.089 1586^{+134}_{-144}	15.911 ± 0.006 1569 ± 79	16.174 ± 0.068 1231^{+97}_{-101}	> 16.300 < 1097
0420-731	...	...	...	...	...	15.450 ± 0.077 2729^{+204}_{-217}	15.507 ± 0.023 2370 ± 87	15.371 ± 0.039 2580^{+158}_{-160}	15.770 ± 0.017 1787 ± 94	... ...
0420+520	...	...	...	...	...	14.873 ± 0.062 4642^{+293}_{-306}	15.009 ± 0.094 3750^{+331}_{-357}	14.833 ± 0.089 4235^{+395}_{-419}	15.195 ± 0.043 3034^{+192}_{-195}	> 15.593 < 2074
0836+404	15.940 ± 0.013 1585 ± 82	15.537 ± 0.015 2214 ± 115	15.775 ± 0.019 1.778 ± 0.094	15.935 ± 0.016 1513 ± 79	16.138 ± 0.016 1239 ± 65	15.842 ± 0.072 1902^{+135}_{-142}	15.636 ± 0.042 2105^{+102}_{-104}	15.591 ± 0.096 2107^{+207}_{-222}	15.795 ± 0.091 1746^{+165}_{-176}	> 16.030 < 1387
1046-017	15.578 ± 0.020 2211^{+118}_{-119}	15.614 ± 0.020 2062 ± 110	15.898 ± 0.015 $1.588^{+0.082}_{-0.083}$	16.104 ± 0.014 1296 ± 67	16.365 ± 0.025 1004 ± 55	15.745 ± 0.023 2079^{+76}_{-77}	15.766 ± 0.036 1867^{+83}_{-84}	15.683 ± 0.043 1936^{+123}_{-125}	15.977 ± 0.057 1476^{+106}_{-109}	... ...
1448+411	16.265 ± 0.018 1175 ± 62	15.873 ± 0.018 1625 ± 86	16.124 ± 0.011 1.290 ± 0.066	16.361 ± 0.015 1022 ± 53	16.613 ± 0.018 800 ± 42	16.073 ± 0.033 1537^{+65}_{-66}	15.931 ± 0.024 1604^{+59}_{-60}	15.903 ± 0.021 1581 ± 85	15.974 ± 0.147 1481^{+202}_{-227}	> 16.486 < 924
2329+407	...	...	...	...	...	13.870 ± 0.032 11694^{+488}_{-496}	13.849 ± 0.027 10915^{+422}_{-427}	13.750 ± 0.034 11482^{+676}_{-682}	14.061 ± 0.042 8622^{+542}_{-550}	14.384 ± 0.078 6316^{+540}_{-567}
Other Selected WDs:										
1146-290	...	...	...	...	...	17.90 ± 0.05 290 ± 20	17.30 ± 0.03 450 ± 20	...	...	...
1330+473	15.035 ± 0.023 3648 ± 199	15.052 ± 0.019 3460^{+183}_{-184}	15.437 ± 0.020 2.428 ± 0.130	15.815 ± 0.024 1691^{+92}_{-93}	16.096 ± 0.017 1287 ± 68	15.229 ± 0.024 3345^{+124}_{-125}	15.233 ± 0.025 3051^{+115}_{-116}	15.108 ± 0.040 3287^{+203}_{-206}	15.503 ± 0.108 2285^{+245}_{-265}	> 15.776 < 1777
2152-548	...	...	...	...	...	14.306 ± 0.016 7826^{+261}_{-262}	14.512 ± 0.037 5927^{+266}_{-271}	14.306 ± 0.016 6881^{+359}_{-360}	14.805 ± 0.021 4345^{+233}_{-234}	> 15.210 < 2992

Table 2—Continued

WD	SDSS: u (mag) (μJy) [0.3543 μm]	g (mag) (μJy) [0.4770 μm]	r (mag) (μJy) [0.6231 μm]	i (mag) (μJy) [0.7625 μm]	z (mag) (μJy) [0.9134 μm]	APASS: B (mag) (μJy) [0.44 μm]	V (mag) (μJy) [0.55 μm]	g (mag) (μJy) [0.4770 μm]	r (mag) (μJy) [0.6231 μm]	i (mag) (μJy) [0.7625 μm]
EXCLUDED – Known WDs with Dust Disks:										
0408-041	···	···	···	···	···	15.640 ± 0.054 2291^{+131}_{-136}	15.513 ± 0.089 2357^{+198}_{-213}	15.512 ± 0.058 2266^{+164}_{-168}	15.794 ± 0.066 1748^{+135}_{-140}	15.944 ± 0.056 1501^{+107}_{-109}
0843+516	15.824 ± 0.032 1764^{+102}_{-103}	15.876 ± 0.022 1621 ± 88	16.234 ± 0.014 1.165 ± 0.060	16.563 ± 0.016 849 ± 44	16.862 ± 0.018 636 ± 34	15.989 ± 0.079 1661^{+127}_{-135}	16.044 ± 0.046 1445^{+74}_{-76}	15.809 ± 0.079 1724^{+149}_{-156}	16.367 ± 0.201 1031^{+182}_{-216}	···
1015+161	15.546 ± 0.021 2278 ± 122	15.465 ± 0.025 2365^{+130}_{-131}	15.800 ± 0.027 $1.738^{+0.097}_{-0.098}$	16.083 ± 0.016 1320 ± 69	16.382 ± 0.026 989 ± 55	15.596 ± 0.043 2385^{+117}_{-120}	15.607 ± 0.061 2162^{+135}_{-141}	15.499 ± 0.040 2293^{+142}_{-144}	15.834 ± 0.077 1684^{+143}_{-150}	> 16.195 < 1.191
1116+026	14.942 ± 0.013 3973 ± 205	14.536 ± 0.024 5568^{+304}_{-305}	14.702 ± 0.019 $4.777^{+0.254}_{-0.255}$	14.956 ± 0.020 3730^{+199}_{-200}	15.194 ± 0.013 2954 ± 152	14.734 ± 0.032 5277^{+220}_{-224}	14.617 ± 0.021 5380^{+191}_{-192}	14.558 ± 0.006 5455 ± 275	14.744 ± 0.014 4596 ± 238	14.957 ± 0.052 3726^{+255}_{-261}
1150-153	···	···	···	···	···	16.110 ± 0.059 1486^{+90}_{-94}	15.963 ± 0.066 1557^{+103}_{-108}	> 15.830 < 1691	> 16.089 < 1332	···
1541+650	15.952 ± 0.020 1567 ± 84	15.550 ± 0.021 2187 ± 117	15.663 ± 0.018 1.972 ± 0.104	15.823 ± 0.014 1678 ± 87	16.108 ± 0.014 1273 ± 66	15.562 ± 0.016 2461 ± 82	15.523 ± 0.006 2336 ± 71	15.412 ± 0.090 2484^{+234}_{-248}	15.621 ± 0.035 2049^{+122}_{-123}	···
1729+371	···	···	···	···	···	···	···	···	···	···
EXCLUDED – WD is a CSPN (central star of a planetary nebula):										
0558-756	···	···	···	···	···	16.207 ± 0.068 1359^{+92}_{-97}	15.303 ± 0.082 2336 ± 71	15.667 ± 0.011 1964 ± 100	14.946 ± 0.040 3816^{+236}_{-239}	14.777 ± 0.016 4398 ± 230
0950+139	15.250 ± 0.068 2992^{+236}_{-245}	15.640 ± 0.035 2014^{+119}_{-121}	16.207 ± 0.018 1.195 ± 0.063	16.515 ± 0.034 887^{+52}_{-53}	16.862 ± 0.028 636 ± 36	15.793 ± 0.027 1990^{+77}_{-78}	15.930 ± 0.038 1605^{+121}_{-129}	15.778 ± 0.038 1773^{+108}_{-109}	16.153 ± 0.080 1256^{+109}_{-115}	···
1821+643	14.257 ± 0.027 7468^{+416}_{-418}	14.732 ± 0.020 4648^{+248}_{-249}	15.258 ± 0.022 2.862 ± 0.155	15.702 ± 0.015 1876 ± 98	16.075 ± 0.023 1312 ± 71	···	···	···	···	···

Table 2—Continued

WD	SDSS: u	g	r	i	z	APASS: B	V	g	r	i
	(mag)	(mag)	(mag)	(mag)	(mag)	(mag)	(mag)	(mag)	(mag)	(mag)
	(µJy)	(µJy)	(µJy)	(µJy)	(µJy)	(µJy)	(µJy)	(µJy)	(µJy)	(µJy)
	[0.3543 µm]	[0.4770 µm]	[0.6231 µm]	[0.7625 µm]	[0.9134 µm]	[0.44 µm]	[0.55 µm]	[0.4770 µm]	[0.6231 µm]	[0.7625 µm]
1958+015	⋯	⋯	⋯	⋯	⋯	⋯	⋯	⋯	⋯	⋯
	⋯	⋯	⋯	⋯	⋯	⋯	⋯	⋯	⋯	⋯
2333+301	⋯	⋯	⋯	⋯	⋯	⋯	⋯	⋯	⋯	⋯
	⋯	⋯	⋯	⋯	⋯	⋯	⋯	⋯	⋯	⋯

[a] WD 1146-290 is too faint for detection by APASS; the tabulated BV photometry is from Bergeron et al. (1997).

Note. — Upper limits are 2σ (95% confidence) levels.

Table 3.   Mid-infrared Photometry of Selected MS99 White Dwarfs

WD	WISE: W1 (mag) (μJy) [3.35 μm]	W2 (mag) (μJy) [4.60 μm]	W3 (mag) (μJy) [11.56 μm]	W4 (mag) (μJy) [22.24 μm]	Spitzer: Types[a]	IRAC-1 (mag) (μJy) [3.550 μm]	IRAC-2 (mag) (μJy) [4.493 μm]	IRAC-3 (mag) (μJy) [5.731 μm]	IRAC-4 (mag) (μJy) [7.872 μm]	MIPS-1 (mag) (μJy) [23.68 μm]
New WD Dust Disk Candidates:										
0249-052	16.468 ± 0.078	15.732 ± 0.149	> 12.819	> 8.981		...	...	...	...	...
	80 ± 6	88^{+11}_{-13}	< 236	< 2138	00000	...	...	...	...	...
0420-731	14.631 ± 0.029	13.974 ± 0.033	11.700 ± 0.112[b]	9.718 ± 0.517[b]		...	...	...	...	...
	435 ± 13	442 ± 15	662^{+66}_{-73}[b]	1084^{+411}_{-662}[b]	00000	...	...	...	...	...
0420+520	14.653 ± 0.039	14.265 ± 0.060	11.492 ± 0.163[b]	8.392 ± 0.235[b]		...	...	...	...	...
	426 ± 17	338^{+19}_{-20}	801^{+112}_{-130}[b]	3678^{+718}_{-890}[b]	00000	...	...	...	...	...
0836+404	15.700 ± 0.057	15.245 ± 0.115	> 12.776	> 8.991		...	...	...	...	...
	162 ± 9	137^{+14}_{-15}	< 246	< 2118	00000	...	...	...	...	...
1046-017	15.836 ± 0.070	15.402 ± 0.123	> 12.208	> 8.753		...	...	...	...	...
	143^{+9}_{-10}	119^{+13}_{-14}	< 414	< 2637	00000	...	...	...	...	...
1448+411	15.890 ± 0.044	15.497 ± 0.082	12.740 ± 0.302	> 9.027		...	...	...	...	...
	136 ± 6	109^{+8}_{-9}	254^{+62}_{-82}	< 2049	00000	...	...	...	...	...
2329+407	13.757 ± 0.027	12.956 ± 0.027	11.520 ± 0.184	> 9.184		...	...	...	...	...
	973 ± 28	1129^{+32}_{-33}	781^{+122}_{-145}	< 1773	00000	...	...	...	...	...
Other Selected WDs:										
1146-290	15.640 ± 0.054	15.327 ± 0.121	> 12.474	> 9.154		...	...	...	...	...
	172 ± 9	127^{+14}_{-15}	< 324	< 1823	00000	...	...	...	...	...
1330+473	16.011 ± 0.058	15.660 ± 0.122	> 13.071	> 9.330		...	...	...	...	...
	122 ± 7	94^{+10}_{-11}	< 187	< 1550	00000	...	...	...	...	...
2152-548	15.555 ± 0.057	15.249 ± 0.121	> 11.990	> 9.075		...	...	...	...	...
	186 ± 10	137^{+15}_{-16}	< 507	< 1960	11110	166 ± 1	106 ± 1	66 ± 1	40 ± 2	...

Table 3—Continued

WD	WISE: W1 (mag) (μJy) [3.35 μm]	W2 (mag) (μJy) [4.60 μm]	W3 (mag) (μJy) [11.56 μm]	W4 (mag) (μJy) [22.24 μm]	Spitzer: Types[a]	IRAC-1 (mag) (μJy) [3.550 μm]	IRAC-2 (mag) (μJy) [4.493 μm]	IRAC-3 (mag) (μJy) [5.731 μm]	IRAC-4 (mag) (μJy) [7.872 μm]	MIPS-1 (mag) (μJy) [23.68 μm]
EXCLUDED – Known WDs with Dust Disks:										
0408-041	13.889 ± 0.028	13.022 ± 0.030	11.565 ± 0.183	> 9.207	11111	...	...	...	...	...
	861^{+25}_{-26}	1062^{+33}_{-34}	749^{+117}_{-138}	< 1736		1024 ± 1	1194 ± 2	1194 ± 2	1118 ± 3	312 ± 21
0843+516	15.898 ± 0.061	15.301 ± 0.108	> 12.159	> 8.815	11110	...	...	...	...	...
	135 ± 8	130^{+12}_{-14}	< 434	< 2490		137 ± 1	127 ± 1	103 ± 2	162 ± 5	...
1015+161	15.521 ± 0.048	14.989 ± 0.083	> 12.252	9.046 ± 0.438	11113	...	...	...	...	...
	192 ± 9	174^{+13}_{-14}	< 398	2014^{+669}_{-1001}		189 ± 1	160 ± 1	139 ± 2	124 ± 4	< 70
1116+026	14.215 ± 0.031	13.788 ± 0.046	12.417 ± 0.541	> 8.827	11112	...	...	...	...	...
	638^{+20}_{-21}	525^{+23}_{-24}	342^{+134}_{-221}	< 2464		589 ± 1	522 ± 1	480 ± 2	459 ± 3	1558 ± 32
1150-153	14.681 ± 0.036	13.736 ± 0.044	12.128 ± 0.386	> 8.645	11110	...	...	...	...	...
	415 ± 15	550^{+23}_{-24}	446^{+134}_{-191}	< 2913		516 ± 2	586 ± 2	614 ± 2	601 ± 4	...
1541+650	14.638 ± 0.027	13.803 ± 0.030	12.928 ± 0.306	> 9.374	00000	...	...	...	...	...
	432^{+12}_{-13}	517 ± 16	214^{+53}_{-70}	< 1489		...	...	...	...	...
1729+371	14.965 ± 0.034	14.144 ± 0.042	11.703 ± 0.140	> 8.955	11111	...	...	...	...	...
	320 ± 11	378^{+15}_{-16}	660^{+80}_{-91}	< 2190		371 ± 1	392 ± 1	422 ± 1	643 ± 2	300 ± 9
EXCLUDED – WD is a CSPN (central star of a planetary nebula):										
0558-756	16.877 ± 0.137	14.677 ± 0.052	10.394 ± 0.046	5.312 ± 0.030	00004	...	...	...	...	...
	55 ± 7	231^{+11}_{-12}	2203^{+97}_{-101}	62743^{+1950}_{-1992}		...	...	...	...	...
0950+139	14.561 ± 0.037	13.543 ± 0.042	9.566 ± 0.042	7.327 ± 0.131	11111	...	...	...	...	...
	464^{+17}_{-18}	657^{+27}_{-28}	4724^{+193}_{-199}	9808^{+1124}_{-1266}		930 ± 3	1151 ± 3	1703 ± 8	3726 ± 9	11853 ± 45
1821+643	16.098 ± 0.034	15.216 ± 0.041	10.933 ± 0.035	6.395 ± 0.036	00000	...	...	...	...	...
	113 ± 4	141 ± 6	1341^{+47}_{-48}	23140^{+830}_{-853}		...	...	...	...	...

Table 3—Continued

WD	WISE: W1 (mag) (μJy) [3.35 μm]	W2 (mag) (μJy) [4.60 μm]	W3 (mag) (μJy) [11.56 μm]	W4 (mag) (μJy) [22.24 μm]	Spitzer: Types[a]	IRAC-1 (mag) (μJy) [3.550 μm]	IRAC-2 (mag) (μJy) [4.493 μm]	IRAC-3 (mag) (μJy) [5.731 μm]	IRAC-4 (mag) (μJy) [7.872 μm]	MIPS-1 (mag) (μJy) [23.68 μm]
1958+015	13.758 ± 0.046 972^{+43}_{-45}	12.360 ± 0.030 1954^{+61}_{-62}	7.621 ± 0.016 28334^{+594}_{-598}	2.684 ± 0.014 705931^{+13897}_{-13974}	00000	…	…	…	…	…
2333+301	16.732 ± 0.105 63 ± 6	15.587 ± 0.127 100^{+11}_{-13}	11.740 ± 0.171 638^{+93}_{-109}	8.130 ± 0.183 4681^{+729}_{-862}	00000	…	…	…	…	…

[a]Spitzer Enhanced Imaging Products Source List (Cryogenic Release v2.0, January 2013) data types for the IRAC-1–4 and MIPS-1 bands, respectively, as follows: 0 = no data available, 1 = flux density measurement (3.8″ diameter aperture for IRAC, PSF-fit for MIPS), 2 = bandfill measurement (i.e., no source detection with S/N>3, so best combined position from detected bands is used to make a flux density measurement), 3 = 3-sigma upper limit (not used here), 4 = extended source, no photometry.

[b]These values should be treated as upper limits – see text for details.

Note. — Upper limits are 2σ (95% confidence) levels. The Spitzer flux density uncertainties do not include systematic error terms, which amount to an additional ≈ 4.5% for IRAC and ≈ 6.5% for MIPS.

Table 4.   Model Parameters for New WD Dust Disk Candidates

WD	Other Name	$T_{\rm eff,wd}$ (K)	distance (pc)	$R_{\rm in,disk}$ ($R_{\rm wd}$)	$R_{\rm out,disk}$ ($R_{\rm wd}$)	inclination (°)	$\tilde{\chi}^2_{\rm wd}$ [a]	$\tilde{\chi}^2_{\rm all}$ [b]	$\tilde{\chi}^2_{\rm disk}$ [c]
0249-052	HE 0245-0514	17823	104	30	52	80	1.3	5.1	1.9
0420-731	$\cdots$	17653	79	18	88	71	2.8	151	6.1[d]
0420+520	KPD 0420+5203	24301	76	12*	28	71	1.4	64	7.8[d]
0836+404	DF Lyn	11712	59	16	86	89	1.0	2.7	1.2
1046-017	GD 124	14266	75	28	38	80	17.6[e]	18.0[e]	17.7[e]
1448+411	CBS 204	13571	80	26	36	80	0.3	9.5	0.9[d]
2329+407	EGGR 160	13900	33	28	68	80	107[e]	155[e]	94[e]
1146-290	Ruiz 440-146	5000	26	$\cdots$	$\cdots$	$\cdots$	12	32	$\cdots$
1330+473	PG	21223	91	$\cdots$	$\cdots$	$\cdots$	461	384	$\cdots$
2152-548	1ES 2152-54.8	45050	123	$\cdots$	$\cdots$	$\cdots$	0.7	10	$\cdots$

* Dust located at $R_{\rm in,disk}$ is at the assumed sublimation temperature.

[a] $\tilde{\chi}^2$ value of the WD model fit compared to only the *GALEX* UV, optical, and 2MASS near-IR data points.

[b] $\tilde{\chi}^2$ value of the WD model fit compared to all available data points.

[c] $\tilde{\chi}^2$ value of the WD + dust disk model fit compared to all available data points.

[d] These values are large due to the inclusion of bright W3 and/or W4 points – see discussion in the text.

[e] Large $\tilde{\chi}^2$ values due to poor fit in the UV – see discussion in the text.

Table 5. Published WD Dust Disk Model Parameters

WD	Other Name	Type[a]	$T_{\rm eff,wd}$ (K)	$R_{\rm in,disk}$ ($R_{\rm wd}$)	$R_{\rm out,disk}$ ($R_{\rm wd}$)	inclination (°)	$T_{\rm subl}$ (K)	Reference	Notes
0106-328	HE 0106-3253	DAZ	15700	15	21	81	...	Farihi et al. (2010)	1
0110-565	HE 0110-5630	DBAZ	19200	31	35	60	1800	Girven et al. (2012)	...
0146+187	GD 16	DABZ	11500	12*	30	48	1200	Farihi et al. (2009)	...
			11500	11	23	26	1000–1500	Jura et al. (2009)	2
0300-013	GD 40	DBZ	15200	18*	44	78	1200	Jura et al. (2007a)	...
			15200	13*	35	81	1000–1500	Jura et al. (2009)	2
0307+077	HS 0307+0746	DAZ	10200	13	17	66	...	Farihi et al. (2010)	1
0408-041	GD 56	DAZ	14400	16*	104	0	1200	Jura et al. (2007a)	...
			14400	10*	71	0	1700	Jura et al. (2007a)	...
			14400	16	45	45	2000	von Hippel et al. (2007)	1
			14400	30	65	41	1000–1500	Jura et al. (2009)	2
0435+410	GD 61	DBAZ	17280	19*	26	79	1300	Farihi et al. (2011)	...
			17500	17	36	85	1800	Girven et al. (2012)	...
J0738+1835	SDSS J073842.56+183509.6	DBZ	13600	9*	25	58	1800	Brinkworth et al. (2012)	...
			13600	12*	21	0	1400	Brinkworth et al. (2012)	...
0842+231[b]	Ton 345	DBZ	18600	17*	100	66	1200–1500	Melis et al. (2010)	...
			18600	13*	187	83	1800	Brinkworth et al. (2012)	...
			18600	19*	100	80	1400	Brinkworth et al. (2012)	...
0843+516	PG; SDSS J084702.28+512853.4	DA	23900	30*	75	82	1200	Xu & Jura (2012)	...
J0959-0200	SDSS J095904.69-020047.6	DAZ	13280	10*	25	0	1200	Farihi et al. (2012)	...
1015+161	PG	DAZ	19300	24*	42	73	1200	Jura et al. (2007a)	...
1041+091[b]	SDSS J104341.53+085558.2	DAZ	18330	23*	80	60	1200–1500	Melis et al. (2010)	...
			17912	13*	14	40	1800	Brinkworth et al. (2012)	...
			17912	18*	38	85	1400	Brinkworth et al. (2012)	...
1116+026	GD 133	DAZ	12200	13*	83	78	1200	Jura et al. (2007a)	...
			12200	12*	50	79	1000–1500	Jura et al. (2009)	2
1150-153	EC11507-1519	DAVZ	12800	10*	30	0	1000–1500	Jura et al. (2009)	2
J1221+1245	SDSS J122150.81+124513.3	DAZ	12250	11*	23	46	1200	Farihi et al. (2012)	...

Table 5—Continued

WD	Other Name	Type[a]	$T_{\rm eff,wd}$ (K)	$R_{\rm in,disk}$ ($R_{\rm wd}$)	$R_{\rm out,disk}$ ($R_{\rm wd}$)	inclination (°)	$T_{\rm subl}$ (K)	Reference	Notes
1226+110[b]	SDSS J122859.92+104033.0	DAZ	22000	18*	107	70	1200–1400	Brinkworth et al. (2009)	⋯
			22020	26	93	73	1200–1500	Melis et al. (2010)	⋯
1349-230	HE 1349-2305	DBAZ	17000	13	35	85	1800	Girven et al. (2012)	⋯
1456+298	G166-58	DAZ	7400	29	⋯	⋯	1200	Farihi et al. (2008)	3
1457-086	PG	DAZ	20400	19*	21	73	1200	Farihi et al. (2009)	⋯
1541+650	KX Dra	DAV	11880	11	32	60	⋯	Kilic et al. (2012)	⋯
J1557+0916	SDSS J155720.77+091624.7	DAZ	22810	25*	52	60	1200	Farihi et al. (2012)	⋯
J1617+1620	SDSS J161717.04+162022.3	WD	13432	9*	20	70	1800	Brinkworth et al. (2012)	⋯
			13432	12*	20	50	1400	Brinkworth et al. (2012)	⋯
1729+371	GD 362	DAZ	9740	12	⋯	⋯	1200	Jura et al. (2007b)	⋯
			9740	6	38	60	2000	von Hippel et al. (2007)	⋯
1929+012	GALEX J193156.8+011745	DAZ	20890	23*	80	70	1350	Debes et al. (2011)	⋯
			23470	25*	40	⋯	1400	Melis et al. (2011)	⋯
2115-560	LTT 8452	DAZ	9700	13	25	80	2000	von Hippel et al. (2007)	⋯
			9700	15	18	53	1200	Farihi et al. (2009)	⋯
			9700	8	30	74	1000–1500	Jura et al. (2009)	2
J2209+1223	SDSS J220934.84+122336.5	DBZ	17300	15*	45	57	1200	Xu & Jura (2012)	4
			17300	20*	60	40	1200	Xu & Jura (2012)	4
2221-165	HE 2221-1630	DAZ	10100	11	21	60	⋯	Farihi et al. (2010)	1
2326+049	G29-38	DAZ	11600	12	22	45	2000	von Hippel et al. (2007)	⋯

Note. — This table does not include the 52 WD dust disk candidates from Debes et al. (2011) – see their Table 7. (1) Published model radii given in units of $R_\odot$; we have assumed $R_{\rm wd} = 0.013$ $R_\odot$. (2) $R_{\rm out,disk}$ is transition radius from optically thick to thin. (3) Possible double degenerate (WD+WD) binary with a circumbinary dust disk. (4) These two disk models have degenerate parameters and produce comparably good fits to the data.

* Dust located at $R_{\rm in,disk}$ is at the assumed sublimation temperature.

[a] WD types from MSonline or SIMBAD.

[b] WD has a gas+dust disk.